Correlation functions of the spin misalignment in magnetic small-angle neutron scattering

Andreas Michels*
Technische Physik, Universität des Saarlandes, Postfach 151150, D-66041 Saarbrücken, Germany
and Physics of Condensed Matter and Advanced Materials, University of Luxembourg,
162A Avenue de la Faïencerie, L-1511 Luxembourg, Luxembourg
(Received 4 May 2010; revised manuscript received 30 June 2010; published 30 July 2010)

We have numerically calculated the autocorrelation function $C(r)$ of the spin misalignment by means of micromagnetic theory. $C(r)$ depends sensitively on the details of the underlying magnetic microstructure and can be determined by Fourier inversion of magnetic small-angle neutron scattering data. The model system which we consider consists of a single isolated spherical nanoparticle that is embedded in an infinitely extended matrix. The particle is uniquely characterized by its magnetic anisotropy field $\mathbf{H}_p(\mathbf{x})$, whereas the matrix is assumed to be otherwise anisotropy-field free. In the approach-to-saturation regime, we have computed the static response of the magnetization to different spatial profiles of $\mathbf{H}_p(\mathbf{x})$. Specifically, we have investigated the cases of a uniform particle anisotropy, uniform core shell, linear increase, and exponential and power-law decay. From the magnetization profiles and the associated $C(r)$, we have extracted the correlation length l_C of the spin misalignment, and we have compared the applied-field dependence of this quantity with semiquantitative theoretical predictions. We find that for practically all of the considered models for the anisotropy field (except the core-shell model) the field dependence of the spin-misalignment fluctuations is quite uniquely reproduced by $l_C(H_i)=\mathcal{L}+l_H(H_i)$, where the field-independent quantity $\mathcal{L}$ is on the order of the particle size and $l_H(H_i)$ represents the so-called exchange length of the applied magnetic field.

DOI: 10.1103/PhysRevB.82.024433 PACS number(s): 61.05.fg, 75.25.−j

I. INTRODUCTION

Small-angle neutron scattering (SANS) is a particularly powerful technique for the investigation of structural inhomogeneities in bulk materials on a length scale between a few nanometers and a few hundred of nanometers. The increasing demand and importance of this method is mainly due to the fact that a wide range of problems in diverse scientific disciplines such as biology, chemistry, physics, and materials science can be tackled. To name only a few, SANS is used to study the vortex lattice in superconductors,[1] precipitates in steels,[2] the magnetic microstructures of nanocrystalline bulk ferromagnets,[3,4] nanoparticles,[5,6] spin glasses,[7] spin-helix chirality and skyrmions in single crystals,[8,9] the magnetization dynamics of ferrofluids,[10] micelle formation in aqueous solution,[11] the fractal structure of volcanic rocks,[12] polymers,[13] or the structure of biological macromolecules.[14,15] For recent reviews in this field, we refer to Refs. 16–21.

The analysis of nuclear and magnetic SANS data usually relies on the so-called particle-matrix concept, which considers small-angle scattering due to a dispersion of particles that are embedded in a matrix of a different phase.[22–24] The SANS signal arises from the difference in the nuclear and magnetic scattering-length densities of particles and matrix. An important quantity is the form factor $F(\mathbf{q})$ of the particle, where $\mathbf{q}$ denotes the momentum-transfer or scattering vector. $F(\mathbf{q})$ contains information on the size and shape of the particle and is known for practically all geometrical shapes. Likewise, several models for the structure factor $S(\mathbf{q})$, which takes into account interparticle interferences/interactions, have been developed (e.g., Ref. 25). Therefore, it may be concluded that within the above particle-matrix picture the theoretical SANS concepts are relatively well developed.

An important class of magnetic materials where this approach fails are nanocrystalline bulk ferromagnets, which can be considered as three-dimensional (3D) dense materials (volume fraction of "particles" $\cong$100%) with an average crystallite size in the 10 nm regime. As is well known, magnetic SANS has its origin in the Fourier image $\mathbf{m}(\mathbf{q})$ of the magnetization vector field $\mathbf{M}(\mathbf{x})$, where $\mathbf{x}$ is the position vector.[26] For bulk magnets, the function $\mathbf{m}(\mathbf{q})$ depends in a complicated way on the magnetic interactions, the most important of which are the (isotropic) exchange interaction, the magnetocrystalline and magnetoelastic anisotropy, the magnetostatic self-interaction, and the Zeeman energy.[27] The ground state of a magnetic material is governed by the competition of these magnetic forces. Besides isotropic exchange, the relatively weak antisymmetric Dzyaloshinskii-Moriya interaction[28,29] gives rise to an additional contribution which prefers nonuniform spin configurations. Due to the broken lattice symmetry at interface regions, the Dzyaloshinskii-Moriya interaction is believed to be particularly relevant in nanomagnetic materials, which are characterized by a large interface-to-volume ratio. This conjecture has recently been supported by experiment.[30,31]

The perturbation in the spin microstructure (spin misalignment) that is caused by a particular type of lattice defect is transmitted by means of the exchange interaction into the surrounding lattice on a characteristic length scale (spin-misalignment length l_C) which falls well into the resolution range of the SANS technique. To a first approximation, l_C depends on the exchange and magnetostatic interaction, on the applied magnetic field, and on the spatial structure of the perturbing magnetic anisotropy field. Clearly, such inhomogeneous magnetization states are not accounted for in the commonly utilized particle-matrix description of magnetic SANS, where mostly magnetically uniform particles are as-

sumed and the structure is treated as a geometrical problem only.

Going beyond particle-matrix concepts, the continuum theory of micromagnetics[32–36] sets the framework for analyzing magnetic microstructures and can be employed for calculating the spin-misalignment SANS cross section $d\Sigma_M/d\Omega$ due to a given magnetization profile $\mathbf{m}(\mathbf{q})$. In a sense, $\mathbf{m}(\mathbf{q})$ may be seen as replacing the particle form factor $F(\mathbf{q})$. The approach of combining SANS and micromagnetics was mainly initiated by Seeger and Kronmüller, who have investigated the influence of spin-misalignment fluctuations due to dislocations on the SANS signal of cold-worked Ni and Fe single crystals.[37–44] We have recently summarized the description of magnetic-field-dependent SANS on nanomagnets in terms of micromagnetic theory.[21]

However, a large fraction of the previous analysis works in reciprocal space and provides closed-form expressions for $d\Sigma_M/d\Omega$, from which parameters such as the exchange-stiffness constant or the mean stray and anisotropy field can be obtained. Since real-space information is missing, the present paper is concerned with the analysis of spin-misalignment fluctuations in the space domain. In particular, we calculate numerically the correlation function $C(r)$ of the spin misalignment for a simple model system which consists of a single isolated nanoparticle that acts as a perturbation for the magnetization of the surrounding matrix. By employing arguments of random anisotropy, we will see that this approach may also describe the behavior of an ensemble of particles. The field dependence of l_C, i.e., of the characteristic range of gradients in the spin structure is obtained for different spatial profiles of the particle's anisotropy field.

The paper is organized as follows. In Sec. II, we briefly sketch the micromagnetic background. Section III provides an introduction into the correlation-function formalism, in particular, we relate the high-field solution for the Fourier coefficient of the magnetization from Sec. II to the correlation function $C(r)$. In Sec. IV, we discuss definitions for extracting the correlation length l_C of the spin misalignment from $C(r)$ data. In Sec. V, we introduce the models for the spatial structure of the magnetic anisotropy field of a single particle, which is embedded in an infinite anisotropy-field-free matrix. In Sec. VI, we present and discuss the results for the magnetization profiles, correlation functions, and for the correlation lengths. The effect of the magnetostatic field, which is neglected in our calculations, is estimated. Section VII summarizes the main results of this study and provides an outlook of future challenges in this direction.

II. MICROMAGNETIC BACKGROUND

In order to achieve a self-contained presentation, we will in this section briefly outline the micromagnetic background which is necessary for the computation of the correlation function of the spin misalignment. A comprehensive discussion of the relation between micromagnetic theory and magnetic neutron scattering can be found in Ref. 21. The static magnetic microstructure, which gives rise to elastic magnetic SANS, obeys the following balance-of-torque equation:[32–36]

$$\left[\frac{2A}{\mu_0 M_s^2}\nabla^2\mathbf{M}(\mathbf{x}) + \mathbf{H}(\mathbf{x}) + \mathbf{H}_p(\mathbf{x})\right] \times \mathbf{M}(\mathbf{x}) = 0. \quad (1)$$

A is the exchange-stiffness constant, $\mu_0 = 4\pi 10^{-7}$ T m/A, $M_s = |\mathbf{M}(\mathbf{x})|$ is the saturation magnetization, $\mathbf{M}(\mathbf{x})$ is the magnetization vector field with Cartesian components $M_x(\mathbf{x}), M_y(\mathbf{x}), M_z(\mathbf{x})$, $\nabla^2\mathbf{M}(\mathbf{x}) = (\nabla^2 M_x, \nabla^2 M_y, \nabla^2 M_z)$, $\mathbf{H}(\mathbf{x})$ is the magnetic field, which is composed of the applied magnetic field $\mathbf{H}_i$ and of the magnetostatic self-interaction field $\mathbf{H}_d(\mathbf{x})$, and $\mathbf{H}_p(\mathbf{x})$ is the magnetic anisotropy field. Note that in the present calculations we assume uniform values for A and M_s. The competition of the various fields in Eq. (1) determines the magnetic microstructure, and at static equilibrium the torque on $\mathbf{M}(\mathbf{x})$ vanishes.

Equation (1) together with boundary conditions represents a system of nonlinear partial differential equations. Therefore, solutions of Eq. (1) and of its dynamic extension, the Landau-Lifshitz-Gilbert equation, are generally only possible by means of numerical micromagnetic computations (e.g., Refs. 45–51). An approximate analytical solution of Eq. (1) is possible at large applied fields, when the variation in the magnetization is confined to the plane perpendicular to $\mathbf{H}_i$. Within this so-called small-misalignment approximation, Eq. (1) can be linearized by ignoring terms which are of higher than linear order in the transversal spin components.

In the following, we focus on the solution of Eq. (1) which is relevant for the SANS geometry where the wave vector $\mathbf{k}_0$ of the incident neutron beam is normal to $\mathbf{H}_i \| \mathbf{e}_z$. For $\mathbf{k}_0 \| \mathbf{e}_x$, the scattering vector (wave vector) $\mathbf{q}$ in the small-angle regime varies exclusively in $\mathbf{e}_y$-$\mathbf{e}_z$ plane, i.e., we can write $\mathbf{q} \cong q(0, \sin\theta, \cos\theta)$, where θ denotes the angle between $\mathbf{q}$ and $\mathbf{H}_i$. Neglecting surface effects, the small-misalignment solution (in the bulk) for the Fourier coefficient $\mathbf{m}(\mathbf{q}) = (m_x, m_y, 0)$ of the reduced transversal magnetization can be expressed as[21,52]

$$m_x(\mathbf{q}) = \frac{h_x(\mathbf{q})}{H_{\mathrm{eff}}(q, H_i)},$$

$$m_y(\mathbf{q}) = \frac{h_y(\mathbf{q})}{H_{\mathrm{eff}}(q, H_i) + M_s \sin^2\theta}, \quad (2)$$

where $h_x(\mathbf{q})$ and $h_y(\mathbf{q})$ represent the Cartesian components of the Fourier transform of the anisotropy field $\mathbf{H}_p(\mathbf{x})$,

$$\mathbf{h}(\mathbf{q}) = \frac{1}{(2\pi)^{3/2}} \int \mathbf{H}_p(\mathbf{x}) \exp(-i\mathbf{q}\cdot\mathbf{x}) d^3x. \quad (3)$$

In the high-field limit, $\mathbf{H}_p(\mathbf{x})$ is assumed to be independent of the magnetization but to depend explicitly on the position $\mathbf{x}$ in the material. The effective magnetic field

$$H_{\mathrm{eff}}(q, H_i) = H_i(1 + l_H^2 q^2) \quad (4)$$

depends on H_i, on $q = |\mathbf{q}|$, and on the exchange length of the field

$$l_H(H_i) = \sqrt{\frac{2A}{\mu_0 M_s H_i}}. \tag{5}$$

The quantity l_H specifies the length scale over which perturbations in $\mathbf{M}(\mathbf{x})$ decay. In particular, l_H represents the correlation length of the spin misalignment when perturbations in the spin microstructure have Delta-function character (see below). The term $M_s \sin^2 \theta$ in Eq. (2) is a consequence of the magnetostatic field $\mathbf{H}_d$ due to nonzero volume divergences of $\mathbf{M}$. In our calculations we have neglected this term, which is justified when $H_{\text{eff}} \gg M_s$ (compare Sec. VI A below). Equation (2) then reduces to the simpler expression

$$\mathbf{m}(\mathbf{q}) \cong \frac{\mathbf{h}(\mathbf{q})}{H_{\text{eff}}(q,H_i)}. \tag{6}$$

The function $\mathbf{m}(\mathbf{q})$ is defined as

$$\mathbf{m}(\mathbf{q}) = \frac{1}{(2\pi)^{3/2}} \int \frac{\mathbf{M}_p(\mathbf{x})}{M_s} \exp(-i\mathbf{q}\cdot\mathbf{x}) d^3x, \tag{7}$$

where $\mathbf{M}_p(\mathbf{x}) = \mathbf{M}(\mathbf{x}) - \langle \mathbf{M} \rangle$ denotes the fluctuation of the magnetization with $\langle \mathbf{M} \rangle$ the mean magnetization, which is parallel to $\mathbf{H}_i$. The reduced transversal magnetization $\mathbf{M}_p(\mathbf{x})/M_s$ is obtained from Eq. (7) using Eq. (6) as

$$\frac{\mathbf{M}_p(\mathbf{x})}{M_s} = \frac{1}{(2\pi)^{3/2}} \int \frac{\mathbf{h}(\mathbf{q})}{H_{\text{eff}}(q,H_i)} \exp(i\mathbf{q}\cdot\mathbf{x}) d^3q. \tag{8}$$

III. CORRELATION FUNCTION OF THE SPIN MISALIGNMENT

The autocorrelation function $C(\mathbf{r})$ of the spin misalignment is defined by close analogy to the well-known Patterson function in x-ray scattering[53] as[54,55]

$$C(\mathbf{r}) = \frac{1}{V} \int \frac{\mathbf{M}_p(\mathbf{x}) \mathbf{M}_p(\mathbf{x}+\mathbf{r})}{M_s^2} d^3x, \tag{9}$$

where V is the sample volume. Note that $C(\mathbf{r})$ is a dimensionless quantity. Alternatively, $C(\mathbf{r})$ may be expressed as

$$C(\mathbf{r}) = \frac{1}{V} \int |\mathbf{m}(\mathbf{q})|^2 \exp(i\mathbf{q}\cdot\mathbf{r}) d^3q. \tag{10}$$

From Eq. (9) it follows, the well-known result, that the value of the correlation function at the origin is equal to the (reduced) mean-square magnetization fluctuation,

$$C(r=0) = \frac{1}{V} \int \frac{|\mathbf{M}_p(\mathbf{x})|^2}{M_s^2} d^3x = \frac{\langle |\mathbf{M}_p|^2 \rangle}{M_s^2}. \tag{11}$$

As was shown, for instance, in Ref. 55, the quantity $C(0)$ can be related to the macroscopic mean magnetization $|\langle \mathbf{M} \rangle|$, which is measured with a magnetometer, according to

$$|\langle \mathbf{M} \rangle| = M_s \sqrt{1 - C(0)}. \tag{12}$$

In the following, we will consider statistically isotropic anisotropy-field microstructures, i.e., $\mathbf{h}(\mathbf{q})$ is assumed to depend only on the magnitude of the wave vector, $\mathbf{h} = \mathbf{h}(q)$ (see discussion in Sec. V). In conjunction with Eq. (6), this implies $\mathbf{m} = \mathbf{m}(q)$ and, hence,

$$C(r,H_i) = \frac{4\pi}{Vr} \int_0^\infty \frac{h^2(q)}{H_{\text{eff}}^2(q,H_i)} \sin(qr) q dq. \tag{13}$$

Likewise, the correlation function can also be obtained from experimental data for the spin-misalignment scattering cross section $d\Sigma_M/d\Omega \propto m^2(q)$, according to[54–56]

$$C(r,H_i) = \frac{K}{r} \int_{q_{\min}}^{q_{\max}} \frac{d\Sigma_M}{d\Omega}(q,H_i) \sin(qr) q dq, \tag{14}$$

where K is a constant and $q_{\min}$ and $q_{\max}$ represent, respectively, the lower and upper limits of the experimentally accessible range of momentum transfers. In a SANS experiment, typically, $q_{\min} \cong 0.01$ nm^{-1} and $q_{\max} \cong 5$ nm^{-1} so that meaningful information on $C(r)$ and, hence, on the spin microstructure can be obtained for distances r within a few nanometers and a few hundred of nanometers, roughly 1–300 nm.

IV. HOW TO EXTRACT THE CORRELATION LENGTH OF THE SPIN MISALIGNMENT?

An important quantity which can be extracted from $C(r)$ is the correlation length l_C of the spin misalignment, which is a measure for the characteristic distance over which perturbations in $\mathbf{M}(\mathbf{x})$ decay. Inspection of Eqs. (3) and (6)–(8) reveals that near saturation the magnetic microstructure in real space, $\mathbf{M}_p(\mathbf{x})/M_s$, corresponds to the convolution of the anisotropy-field microstructure $\mathbf{H}_p(\mathbf{x})$ with an exponential which decays with the characteristic length l_H. Therefore, from this point of view, it seems quite reasonable to assume that in the approach-to-saturation regime l_C depends on l_H and on a characteristic (field-independent) length scale $\mathcal{L}$, which is related to the magnetic anisotropy field, i.e., to the size of the defect (see discussion below). For comparison, in nuclear SANS, the correlation function of a single uniform sphere with radius R reads[57] $C(r) = 1 - 3r/(4R) + r^3/(16R^3)$ for $r \leq 2R$ and $C = 0$ for $r > 2R$. Applying, for instance, the definition Eq. (16) (see below) yields a correlation length of $l_C = \frac{4}{3}R$.

However, in contrast to nuclear SANS studies on polydisperse particle assemblies, where microstructural parameters such as, for instance, the radius of gyration or the correlation length may be obtained from certain ratios of moments of the measured scattering intensity (e.g., Ref. 58), it is not immediately obvious how to extract l_C from magnetic SANS data. This difficulty arises mainly because l_C is a field-dependent quantity which characterizes the magnetic microstructure and, therefore, by virtue of the above-mentioned convolution property, l_C is closely related (via $\mathbf{H}_p$) to the nuclear grain microstructure.

In Refs. 54 and 55, we have suggested the following two definitions for extracting l_C from $C(r)$ curves, which can be obtained from magnetic-field-dependent SANS data. First, we have identified l_C with the r value for which the extrapolated value of $C(r)$ to the origin, $C(0)$, has decayed to $C(0)\exp(-1)$, i.e.,

$$l_C = r \quad \text{for which} \quad C(r) = C(0)\exp(-1). \tag{15}$$

Second, we have determined l_C by means of the logarithmic derivative of $C(r)$ in the limit $r \to 0$, i.e.,

$$l_C = -\lim_{r\to 0}\left(\frac{d\ln C}{dr}\right)^{-1}. \tag{16}$$

Both definitions for l_C, Eqs. (15) and (16), do not require that $C(r)$ is an exponential, but they yield the exact correlation length when the correlations decay exponentially. We would also like to note that within the present micromagnetic approach exponentially decaying correlation functions are rather the exception than the rule. For the here considered models for $\mathbf{H}_p(\mathbf{x})$ (except the Delta-function perturbation), the numerical calculations reveal that in the limit $r \to 0$ the slope of $C(r)$ vanishes [compare, e.g., Figs. 2(b), 5, 7, and 10 below]. This result is consistent with the lack of a sharp boundary in the magnetic microstructure (infinitely extended magnetization profiles) and with the absence of an asymptotic q^{-4} Porod behavior (see Sec. V F).[57] Therefore, the definition Eq. (16) is not used in the following. We would also like to note that an alternative route to extracting a spin-misalignment length may be realized by the computation of moments of the correlation function.[59]

V. MODELS FOR THE ANISOTROPY-FIELD MICROSTRUCTURE

In this section, we will introduce some simple models for the anisotropy field $\mathbf{H}_p(\mathbf{x})$ which will be used for the later calculation of the reduced transversal magnetization and of the correlation function of the spin misalignment. In particular, we consider a single isolated particle with a given anisotropy field which is embedded in an infinitely extended anisotropy-field-free matrix. For simplicity, we assume the particle to be a sphere of radius R_1. Additionally, we consider a core-shell particle with inner radius R_1 and outer radius R_2. Figure 1 displays the different models for the anisotropy field.

We would like to particularly note that the above assumption of a single isolated particle is not as "severe" as the comparable assumption in nuclear SANS, where the application of single-particle form factors is restricted to dilute systems and implies the neglect of interparticle interference. Here, we consider magnetic microstructures that contain many lattice imperfections, for instance, many crystallites separated by grain boundaries, which are arranged so that the orientation and/or magnitude of their individual anisotropy fields are statistically uncorrelated (random anisotropy). When the orientations of the $\mathbf{h}_i$ are uncorrelated, then terms $\mathbf{h}_i \cdot \mathbf{h}_j$ with $i \neq j$ will appear with either sign with equal probability, and the expectation value for their sum vanishes. Consequently, the expectation value for the magnitude square of the total anisotropy-field Fourier coefficient $|\mathbf{h}(\mathbf{q})|^2 = |\Sigma_i \mathbf{h}_i(\mathbf{q})|^2$ decomposes into the sum of the magnitude squares of the anisotropy fields of the individual defects, i.e., $|\mathbf{h}(\mathbf{q})|^2 = \Sigma_i |\mathbf{h}_i(\mathbf{q})|^2$. Within the validity of the linear approximation, i.e., $\mathbf{m}(\mathbf{q}, H_i) = \mathbf{h}(\mathbf{q}) / H_{\text{eff}}(q, H_i)$, the above property of $|\mathbf{h}(\mathbf{q})|^2$ also transfers to $|\mathbf{m}(\mathbf{q})|^2$ and, hence, to the ensuing spin-misalignment scattering cross section $d\Sigma_M / d\Omega$. In other words, in order to obtain results which are representative for the entire microstructure, it is (within the assumption of random anisotropy) sufficient to solve the single-grain problem.[52]

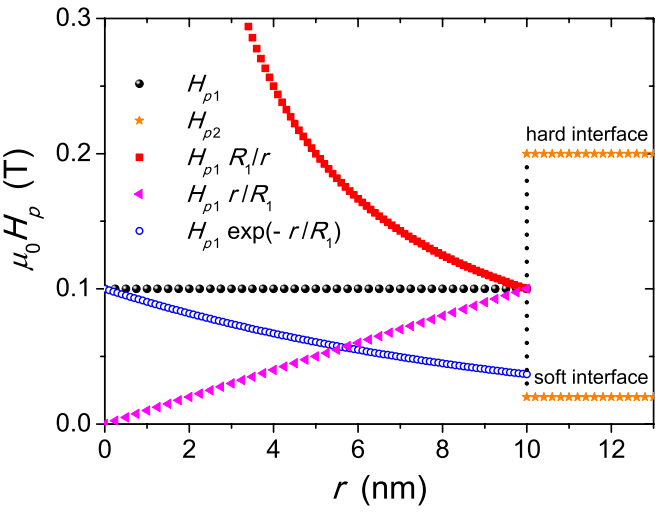

FIG. 1. (Color online) Models for the spatial structure of the magnetic anisotropy field $\mathbf{H}_p(|\mathbf{x}|=r)$ of a spherical particle (core shell), which is embedded in an anisotropy-field-free matrix. For illustration purposes, we have chosen $R_1 = 10$ nm, $R_2 = 13$ nm, $\mu_0 H_{p1} = 0.1$ T, and $\mu_0 H_{p2} = 0.2$ T (0.02 T).

A. Uniform sphere

One of the simplest models for $\mathbf{H}_p(\mathbf{x})$ is a uniform sphere, where the anisotropy field of the sphere, $\mathbf{H}_{p1}$, is assumed to be a constant vector that points into an arbitrary direction in space. Note that the magnitude H_{p1} of the anisotropy field is on the order of K_1/M_s, where K_1 denotes an anisotropy constant. The relation between the Fourier coefficients $\mathbf{h}(\mathbf{q})$ and $\mathbf{H}_p(\mathbf{x})$, Eq. (3), then allows one to compute $h(q)$. The result for $h^2(q)$ is

$$h^2(q, R_1) = \frac{H_{p1}^2}{(2\pi)^3} F^2(q, R_1), \tag{17}$$

where $F(q, R_1)$ is defined as

$$F(q, R_1) = 3V_1 \frac{[\sin(qR_1) - qR_1 \cos(qR_1)]}{(qR_1)^3} \tag{18}$$

and $V_1 = \frac{4}{3}\pi R_1^3$ denotes the volume of the sphere.

B. Uniform core shell

A straightforward extension of the uniform-sphere model is the uniform core-shell model, where the anisotropy fields of the core, $\mathbf{H}_{p1}$, and of the shell, $\mathbf{H}_{p2}$, are both constant vectors but with different magnitudes. For $h^2(q)$, we obtain

$$h^2(q,R_1,R_2) = \frac{H_{p1}^2}{(2\pi)^3}F^2(q,R_1) + \frac{H_{p2}^2}{(2\pi)^3}[F(q,R_2) - F(q,R_1)]^2 + \frac{2H_{p1}H_{p2}\cos\psi}{(2\pi)^3}F(q,R_1)[F(q,R_2) - F(q,R_1)], \tag{19}$$

where ψ denotes the angle between $\mathbf{H}_{p1}$ and $\mathbf{H}_{p2}$ and $V_2 = \frac{4}{3}\pi R_2^3$. The above expression for $h^2(q)$, Eq. (19), may be able to model the effect of an interface anisotropy. Depending on the relative magnitudes of H_{p1} and H_{p2}, one may distinguish between magnetically "hard" ($H_{p1}/H_{p2} < 1$) and "soft" ($H_{p1}/H_{p2} > 1$) interfaces.

C. Exponential decay

For an exponentially decaying anisotropy field with a characteristic length scale R_1, i.e., $\mathbf{H}_p(|\mathbf{x}|=r) = \mathbf{H}_{p1}\exp(-r/R_1)$ with $\mathbf{H}_{p1}$=constant, we obtain for the magnitude square of the anisotropy-field Fourier coefficient

$$h^2(q,R_1) = \frac{2H_{p1}^2R_1^4}{\pi e^2 q^2(1+q^2R_1^2)^4} \times [qR_1\cos(qR_1)(3+q^2R_1^2) + 2\sin(qR_1) - 2eqR_1]^2. \tag{20}$$

D. Power-law decay

When the anisotropy field decays according to a power law, $\mathbf{H}_p(r) = \mathbf{H}_{p1}(R_1/r)^n$ with $\mathbf{H}_{p1}$=constant, we obtain (for $n=1$)

$$h^2(q,R_1) = \frac{2H_{p1}^2R_1^2[1-\cos(qR_1)]^2}{\pi q^4}. \tag{21}$$

Note that the above expression for $\mathbf{H}_p$ diverges as $r \to 0$ and that H_p takes on the value of H_{p1} at the interface ($r=R_1$). In our computations, we have also used $\mathbf{H}_p(r) = \mathbf{H}_{p1}[R_1/(R_1+r)]^n$ with $n \geq 1$, which is finite at $r=0$. The results for the corresponding magnetization profiles and correlation functions are qualitatively similar to the above case of Eq. (21), and the values for the correlation length of the spin misalignment are nearly identical.

E. Linear increase

When $\mathbf{H}_p$ increases linearly from $r=0$ to $r=R_1$, i.e., $\mathbf{H}_p(r) = \mathbf{H}_{p1}(r/R_1)$ with $\mathbf{H}_{p1}$=constant, we obtain

$$h^2(q,R_1) = \frac{2H_{p1}^2}{\pi R_1^2 q^8}[2qR_1\sin(qR_1) + (2-q^2R_1^2)\cos(qR_1) - 2]^2. \tag{22}$$

F. Delta-function perturbation

Finally, we note that for a Delta-function-type perturbation, $\mathbf{H}_p(\mathbf{x}) \propto \delta(\mathbf{x})$, the anisotropy-field Fourier coefficient is a constant, and we obtain the familiar result that the spin-misalignment fluctuations decay exponentially, i.e., $C(r) \propto \exp(-r/l_C)$. The resulting scattering is described by a Lorentzian-squared function with the correlation length $l_C(H_i) = l_H(H_i)$. This result is perfectly reproduced by our algorithm. By contrast, all the other models for $\mathbf{H}_p(\mathbf{x})$ yield asymptotically $h^2(q) \propto q^{-4}$. In conjunction with the q^{-4} dependence of H_{eff}^{-2}, this results in spin-misalignment scattering cross sections $d\Sigma_M/d\Omega$ which may be as steep as q^{-8} (Ref. 21).

VI. RESULTS AND DISCUSSION

For the computation of the magnetization and correlation functions, we have used the materials parameters of Ni (Ref. 21): $A = 8.2 \times 10^{-12}$ J/m and $M_s = 500$ kA/m ($\mu_0 M_s = 0.628$ T). The radius of the sphere was taken as $R_1 = 10$ nm, and for the core shell we have assumed $R_1 = 10$ nm and $R_2 = 13$ nm. Moreover, unless stated otherwise, the magnitudes of the anisotropy fields of the sphere and of the magnetically hard shell were, respectively, chosen as $\mu_0 H_{p1} = 0.1$ T and $\mu_0 H_{p2} = 1.0$ T. The integrals for M_p/M_s and for $C(r)$, Eqs. (8) and (13), have both been solved numerically using Gauss-Legendre integration.

A. Influence of the magnetostatic field

As mentioned in Sec. II, we have neglected in our computations the effect of the magnetostatic field, i.e., we have solved the simpler Eq. (6) rather than Eq. (2), which calls for a twofold numerical integration. This simplification is based on the general notion that demagnetizing effects are expected to be negligible in the approach-to-saturation regime. In order to check whether this assumption is justified or not, we have calculated $\frac{M_p}{M_s}(r)$ and $C(r)$ taking into account $\mathbf{H}_d$ and compared the results with the situation when the term $M_s \sin^2\theta$ in Eq. (2) is neglected. For this computation, we have assumed that the anisotropy field of the particle increases linearly from the origin to the interface, $\mathbf{H}_p(r) = \mathbf{H}_{p1}(r/R_1)$; in order to assure that $|\mathbf{H}_{p1}| = H_{p1}$, we have taken $\mathbf{H}_{p1} = H_{p1}(1/\sqrt{2}, 1/\sqrt{2}, 0)$. The results of such an analysis are shown in Fig. 2.

Several observations may be noted. First, since the inclusion of the magnetostatic field suppresses $\mathbf{m}(\mathbf{q})$ [compare Eq. (2)], both M_p/M_s and C at a given field are larger without $\mathbf{H}_d$ [solid lines in Figs. 2(a) and 2(b)] than with $\mathbf{H}_d$ (dashed lines). Second, the difference between the two cases becomes progressively smaller as the applied field is increasing, thus, corroborating that demagnetizing-field effects are indeed negligible at the larger fields, here, for $\mu_0 H_i \gtrsim 1$ T. Third, the shapes of the $\frac{M_p}{M_s}(r)$ and $C(r)$ curves are very similar and the resulting values for the correlation length l_C of the spin misalignment are almost identical [Fig. 2(c)]. Therefore, we have neglected in our study the term due to $\mathbf{H}_d$.

In the following, we will present a more thorough discussion of the magnetization profiles and correlation functions.

B. Magnetization profiles and correlation functions

Figure 3 displays the results for the applied-field dependence of the magnitude of the reduced transversal magnetization M_p/M_s. As expected, an increasing applied field sup-

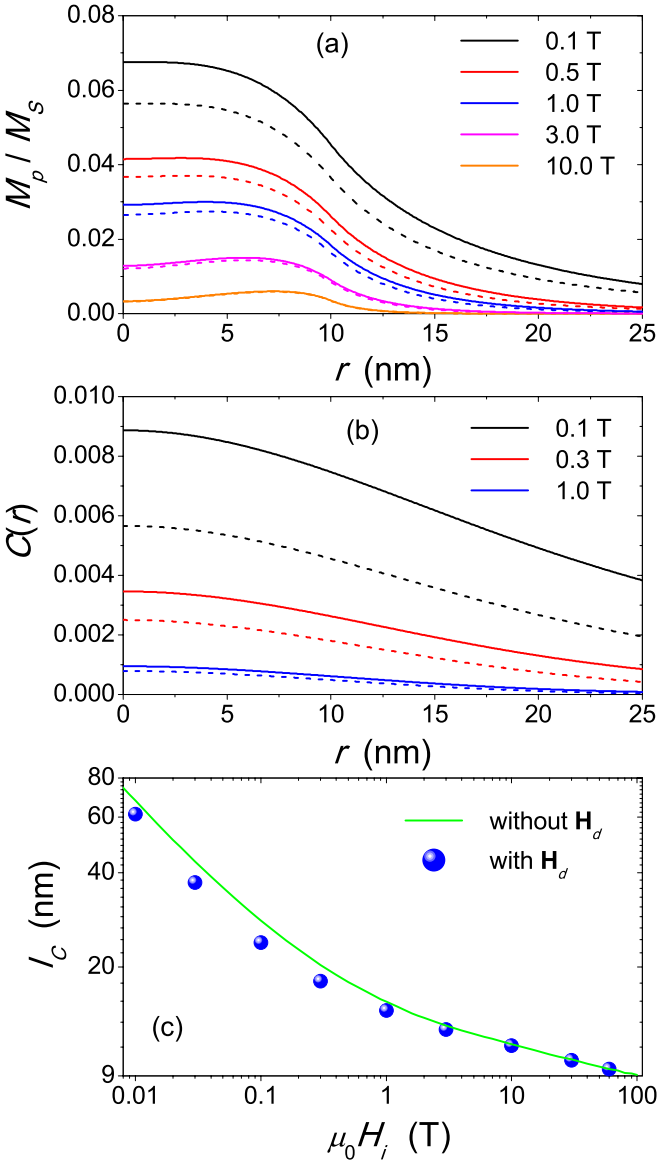

FIG. 2. (Color online) (a) Magnetization profiles $\frac{M_p}{M_s}(r)$ and (b) correlation functions $C(r)$ of the spin misalignment for the case that the particle's anisotropy field increases linearly, $\mathbf{H}_p(r)=\mathbf{H}_{p1}(r/R_1)$ with $\mu_0 H_{p1}=0.1$ T and $R_1=10$ nm. Values of the applied magnetic field are indicated in the insets and increase from top to bottom, respectively. Solid lines: no magnetostatic field. Dashed lines: with magnetostatic field. (c) Field dependence of l_C (log-log scale) obtained by ignoring $\mathbf{H}_d$ (solid line) and by taking into account $\mathbf{H}_d$ (●); l_C was determined by means of Eq. (15).

presses spin fluctuations. The M_p/M_s curves reveal that the perturbation which is caused by the anisotropy-field distribution of the particle is largest at the center of the dominating defect, and then M_p/M_s decays smoothly at the larger distances. While the data for the uniform-sphere model [Fig. 3(a)] and the exponential decay case [Fig. 3(c)] are qualitatively similar, the shapes of the other two M_p/M_s curves are significantly different: the core-shell particle [Fig. 3(b)] exhibits a peak in M_p/M_s due to the hard shell (see below), and for the power-law decay case [Fig. 3(d)], we find an almost linear decrease in M_p/M_s at small r and not too large fields.

The results in Fig. 3 also demonstrate the special role of the exchange length l_H, which can be taken as the spatial resolution limit of the magnetization.[60] In the small-misalignment approximation, variations in the magnetic anisotropy field on a characteristic microstructural length scale $\mathcal{L}$ can be followed by the magnetization only when $l_H \lesssim \mathcal{L}$. At the largest fields, l_H is on the order of a few nanometer, e.g., $l_H(5\ \mathrm{T}) \cong 2.6$ nm for Ni and sharp variations in M_p/M_s on a scale on the order of l_H can be resolved. This can be clearly seen, for instance, in Fig. 3(b), where the perturbing effect of the magnetically hard shell (located at $R_1 \le r \le R_2$) is only seen at the largest field values, and it gives rise to a peak feature which is washed out at the lower fields. A similar behavior is also found when the particle's anisotropy field increases linearly from the origin to the interface [compare Fig. 2(a)].

Note that the validity of the present approach is restricted to large applied fields in order to guarantee that $M_p/M_s \ll 1$. For the core-shell particle with hard interfaces, inspection of Figs. 3(b) and 4 suggests that (for the assumed parameter values) this small-misalignment criterion is fulfilled for fields larger than a few tesla; for the other models, much smaller fields are required in order to satisfy $M_p/M_s \ll 1$.

The effect of the angle ψ between $\mathbf{H}_{p1}$ and $\mathbf{H}_{p2}$ on the magnetization distribution of the hard core-shell particle is seen in Fig. 4. As expected, for a fixed external field, the transversal magnetization decreases at the smallest distances when ψ is increased from 0° (parallel orientation) to 180° (antiparallel orientation). Variations in ψ also affect the corresponding correlation functions and spin-misalignment lengths (not shown). However, the results for the $C(r)$ and $l_C(H_i)$ are qualitatively very similar and the quantitative differences are relatively small, for instance, l_C at 10 T decreases only by about 3 nm when ψ varies between $\psi=0°$ and $\psi=180°$. Therefore, we consider in the following only the case that $\mathbf{H}_{p1}$ is parallel to $\mathbf{H}_{p2}$ ($\psi=0°$).

In agreement with the M_p/M_s curves, the corresponding correlation functions shown in Fig. 5 are strongly field dependent and reveal the long-range nature of the spin-misalignment fluctuations. Despite the existing differences in the underlying functional dependencies of $\mathbf{H}_p(\mathbf{x})$ and the associated M_p/M_s data (compare Fig. 3), the shapes of the different $C(r)$ in Fig. 5 appear to be closely similar: for the anisotropy-field microstructures investigated in this study, $C(r)$ at a given field takes on the maximum value at $r=0$ with $(dC/dr)_{r\to 0}=0$ and then decays toward $C=0$ for $r\to\infty$. Clearly, the correlations do neither decay exponentially nor according to the Ornstein-Zernike formula.

The field dependencies of the corresponding mean-square magnetization fluctuations are displayed in Fig. 6. Except for the core-shell model, the $C(0)$ curves are very similar. For the power-law decay case, the following closed-form expression for $C(0)$ could be derived from Eqs. (6), (10), and (21) (solid line in Fig. 6):

$$C(r=0,H_i)=\frac{3H_{p1}^2}{2R_1H_i^2}\exp(-R_1/l_H)[(2R_1+6l_H)+(R_1-6l_H)\times\cosh(R_1/l_H)+(3R_1-3l_H)\sinh(R_1/l_H)]. \quad (23)$$

Equation (23) describes the approach-to-saturation behavior

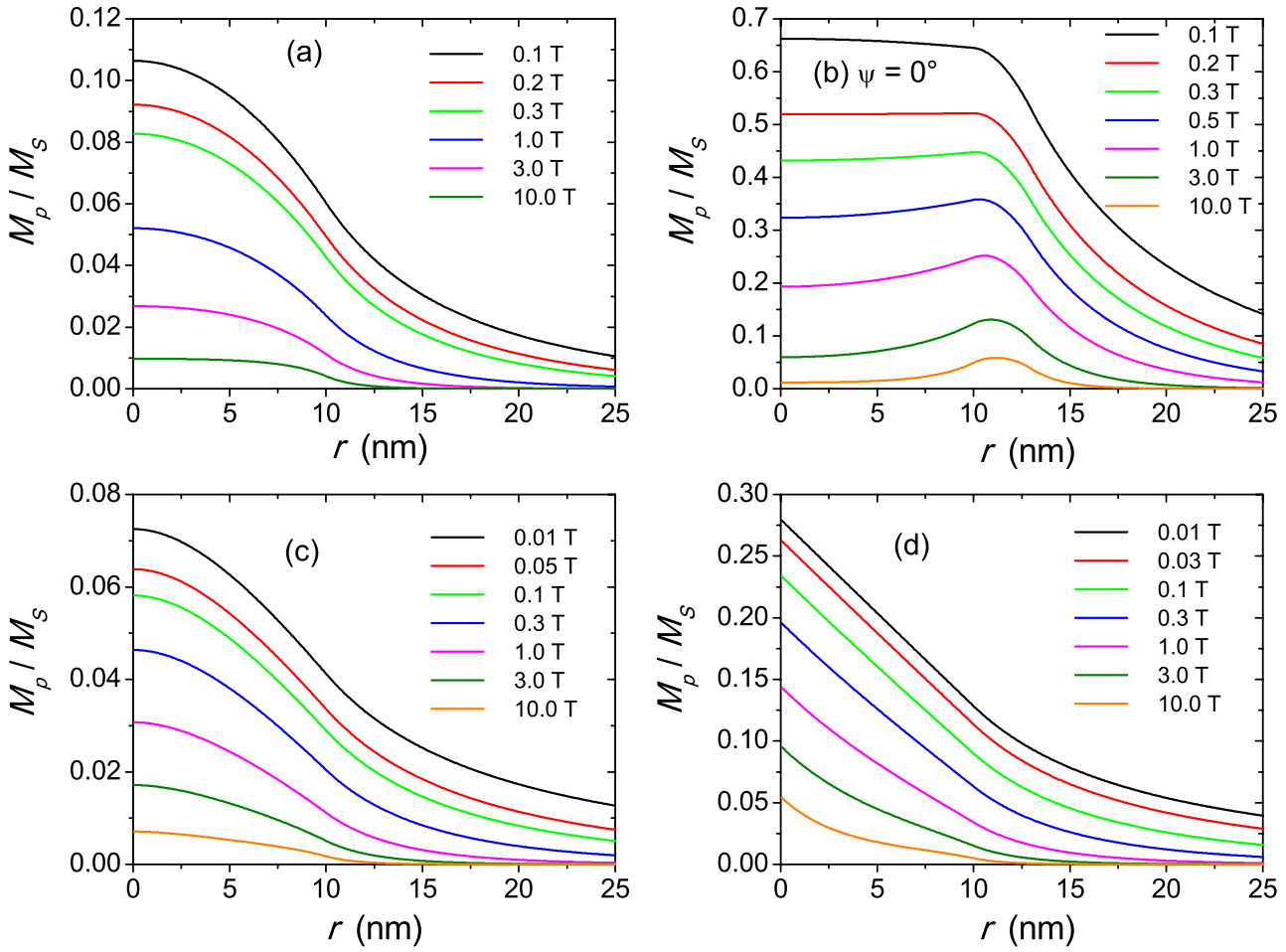

FIG. 3. (Color online) Reduced transversal magnetization component M_p/M_s as a function of the distance r from the center of the inclusion. Values of the applied magnetic field are indicated in the insets and increase from top to bottom, respectively. (a) uniform-sphere model ($R_1=10$ nm, $\mu_0 H_{p1}=0.1$ T). (b) Uniform core-shell model with hard interfaces ($R_1=10$ nm, $R_2=13$ nm, $H_{p1}/H_{p2}=0.1$, and $\psi=0°$). (c) Exponential decay. (d) Power-law decay.

[compare Eq. (12)]. Closed-form expressions for $C(0)$ can also be found for the uniform-sphere model and the uniform core-shell model, and for the case of a linear increase in $\mathbf{H}_p(\mathbf{x})$. However, these expressions are rather lengthy and we prefer not to display them explicitly.

Closer inspection of the data in Fig. 5(b) reveals, however, that the $C(r)$ of the uniform core-shell model with hard interfaces change their curvature twice while the other correlation functions, which contain the single microstructural length scale R_1, change their curvature only once. This observation is depicted in Fig. 7, where we show the correlation functions along with their derivatives $dC(r)/dr$ for the uniform-sphere model at 0.7 T and for the uniform core-shell model at 10.0 T. We suggest that the origin of the two minima in the dC/dr data of the core-shell model at large fields is related to the presence of two types of "defects" in the microstructure: the first defect of strength H_{p1} is represented by the anisotropy field of the core of the particle while the second defect is identified with the hard shell ($H_{p1}/H_{p2}=0.1$). At large applied fields, the correlation functions of the uniform core-shell model reveal a relatively steep decrease at small distances, which is followed by a slower decrease at the larger r [compare Figs. 7 and 10(b) below]. This behavior

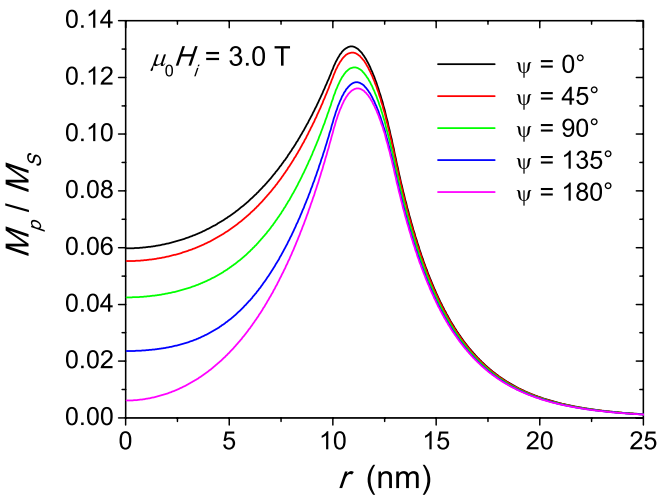

FIG. 4. (Color online) M_p/M_s for the uniform core-shell model with hard interfaces at an applied magnetic field of $\mu_0 H_i=3.0$ T and for different angles ψ between $\mathbf{H}_{p1}$ and $\mathbf{H}_{p2}$ ($R_1=10$ nm, $R_2=13$ nm, and $H_{p1}/H_{p2}=0.1$). Values of ψ are given in the inset and increase from top to bottom.

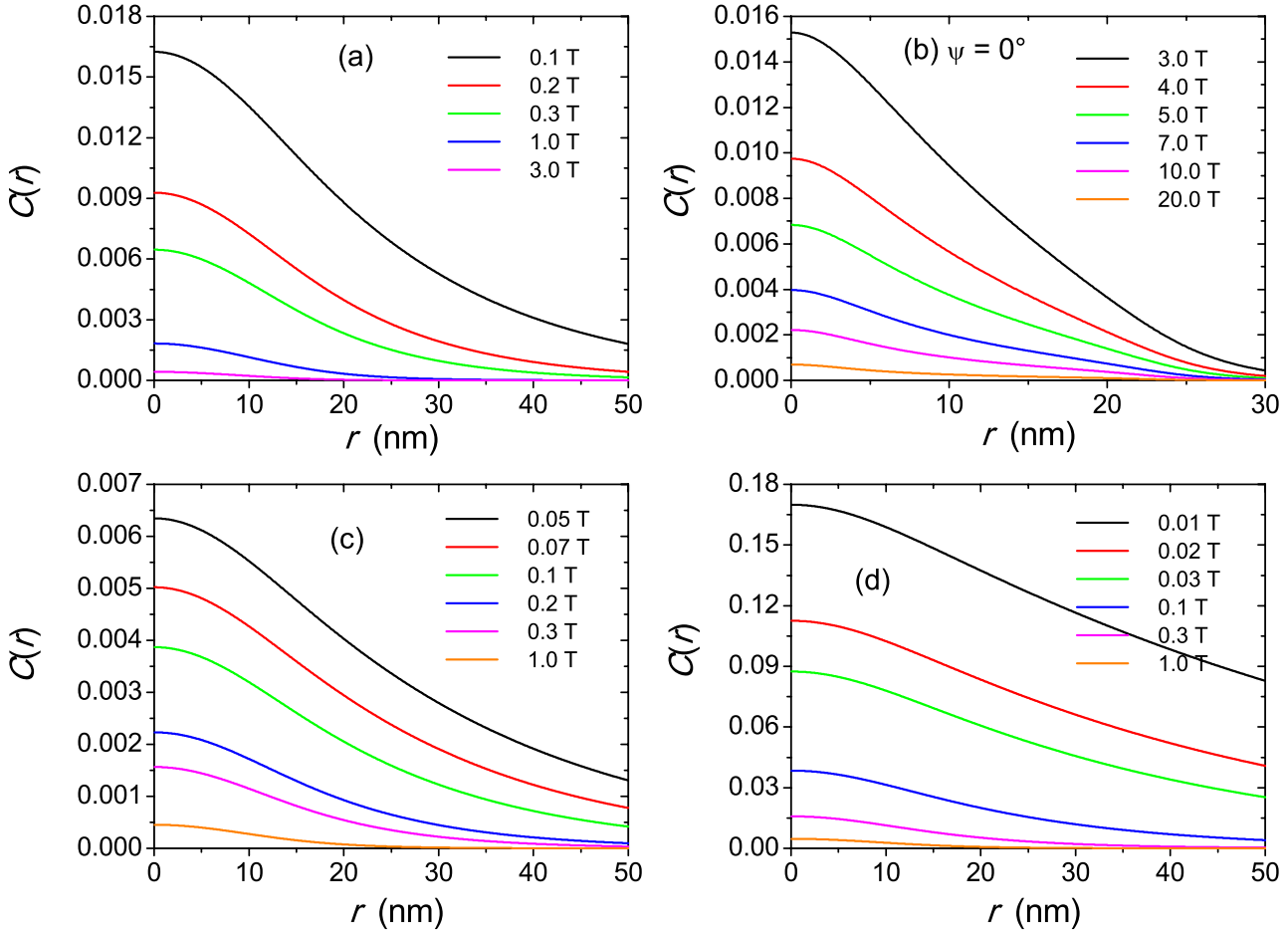

FIG. 5. (Color online) Results for the field dependence of the correlation function $C(r)$ of the spin misalignment. Values of the applied magnetic field are indicated in the insets and increase from top to bottom, respectively. (a) Uniform-sphere model (R_1=10 nm and $\mu_0 H_{p1}$=0.1 T). (b) Uniform core-shell model with hard interfaces (R_1=10 nm, R_2=13 nm, H_{p1}/H_{p2}=0.1, and ψ=0°). (c) Exponential decay. (d) Power-law decay.

can be understood by inspection of the corresponding magnetization profiles [Figs. 3(b) and 4] and by the definition of the correlation function, Eq. (9).

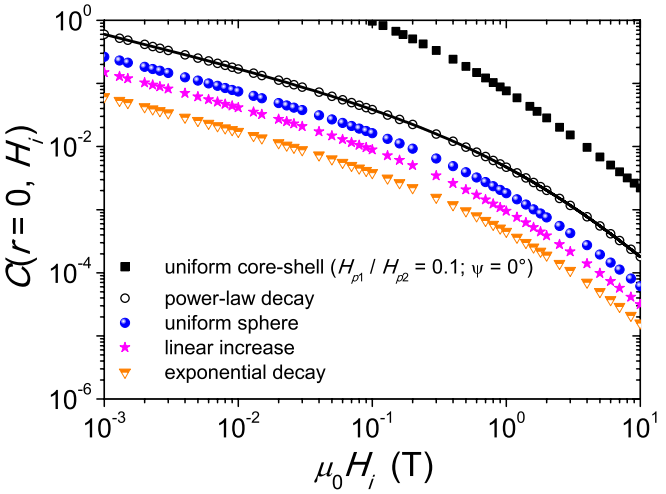

FIG. 6. (Color online) Field dependence of the mean-square magnetization fluctuation $C(r=0,H_i)$ (log-log scale). Solid line: Eq. (23).

We have attempted to "exploit" the above circumstance for determining field-dependent correlation lengths of the spin misalignment by identifying the l_C's with the r values at which the respective dC/dr exhibits minima. It turned out that this procedure leads to difficulties in locating the exact positions of the minima in dC/dr, in particular, for the second minimum at the larger distances, since this feature becomes progressively less pronounced at the smaller values of the applied field (compare, e.g., the minimum in dC/dr at $r \cong 21.5$ nm in Fig. 7). Therefore, we have employed the definition Eq. (15) for determining a single characteristic correlation length from the correlation functions shown in Fig. 5.

C. Correlation length of the spin misalignment

The results for the field dependence of l_C for the different models for $\mathbf{H}_p(\mathbf{x})$ can be seen in Fig. 8. Surprisingly, we find that the simple function

$$l_C(H_i) = \mathcal{L} + l_H(H_i) \tag{24}$$

with $\mathcal{L}=R_1=10$ nm [solid line in Fig. 8(a)] provides a very good description of the l_C data for practically all the consid-

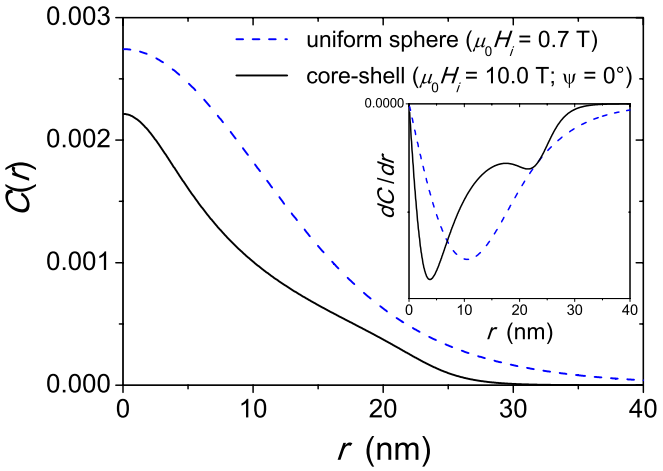

FIG. 7. (Color online) Correlation functions $C(r)$ of the spin misalignment for the uniform-sphere model (R_1=10 nm and $\mu_0 H_{p1}$=0.1 T) and for the uniform core-shell model with hard interfaces (R_1=10 nm, R_2=13 nm, H_{p1}/H_{p2}=0.1, and ψ=0°). Inset: respective derivatives dC/dr.

ered functional dependencies of the anisotropy field, except the core-shell model [see Fig. 8(b)], which exhibits a more complicated behavior $l_C(H_i)$. The choice $l_C(H_i)=\mathcal{L}+l_H(H_i)$ is motivated by the above-mentioned convolution property (compare discussion in Sec. IV), where the quantity $\mathcal{L}$ is on the order of the defect size. Likewise, the function $l_C=\sqrt{\mathcal{L}^2+l_H^2}$ with $\mathcal{L}=R_1$ [dashed line in Fig. 8(a)] also reasonably reproduces the field dependence of l_C. As expected, the core-shell model with soft interfaces (H_{p1}/H_{p2}=10) exhibits an almost identical field dependence $l_C(H_i)$ as the uniform-sphere model or as the cases of exponential or power-law

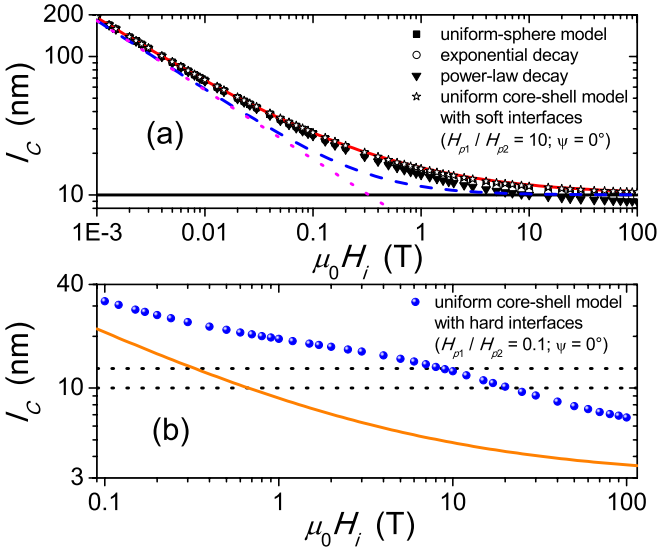

FIG. 8. (Color online) Results for the field dependence of the correlation length l_C of the spin misalignment (log-log scale). l_C was determined by means of the definition Eq. (15). Solid line in (a): $l_C(H_i)=R_1+l_H(H_i)$. Dashed line in (a): $l_C(H_i)=\sqrt{R_1^2+l_H^2(H_i)}$. Dotted line in (a): $l_C(H_i)=l_H(H_i)$. Solid horizontal line in (a): $l_C=R_1$=10 nm. Solid line in (b): $l_C(H_i)=\Delta R+l_H(H_i)$. Dotted horizontal lines in (b): R_1=10 nm and R_2=13 nm.

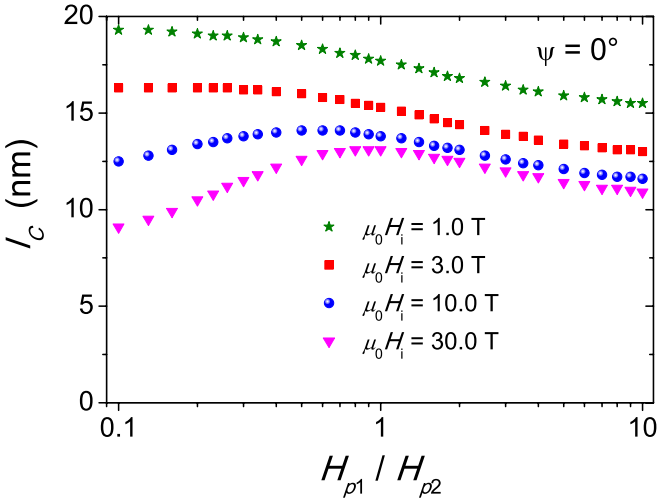

FIG. 9. (Color online) l_C for the uniform core-shell model as a function of the ratio H_{p1}/H_{p2} (log-linear scale) and at different applied magnetic fields (see inset) (R_1=10 nm, R_2=13 nm, and ψ=0°). l_C was determined by means of Eq. (15).

decay. Quite uniquely and irrespective of the internal structure of the anisotropy field of the particle, we find a value of l_C which is close to R_1 at the largest fields. It is also demon-

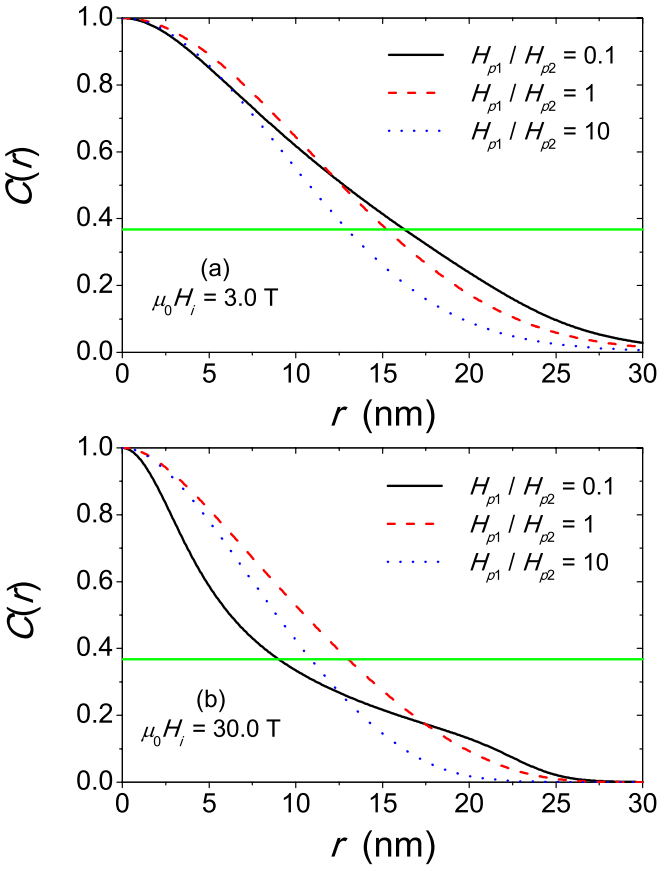

FIG. 10. (Color online) Normalized correlation functions $C(r)$ of the spin misalignment for the uniform core-shell model at two different applied magnetic fields and as a function of the ratio H_{p1}/H_{p2} (see insets) (R_1=10 nm, R_2=13 nm, and ψ=0°). (a) $\mu_0 H_i$=3.0 T and (b) $\mu_0 H_i$=30.0 T. Solid horizontal lines in (a) and (b): $C(r)$=exp(−1).

strated in Fig. 8(a) that exponentially decaying magnetization fluctuations, which result in $l_C = l_H$ (dotted line), are not in accordance with Eq. (24) already at fields larger than a few 10 mT.

The field dependence of l_C for the uniform core-shell model with hard interfaces [Fig. 8(b)] is significantly different from the $l_C(H_i)$ of all the other models for $\mathbf{H}_p(\mathbf{x})$ [Fig. 8(a)] and cannot be described by the simple relation Eq. (24). At the largest fields, it can be seen that l_C exhibits a tendency to evolve on a length scale which is significantly smaller than the radius of the core-shell particle. However, in a field regime which is realistically achieved in experiment, $\mu_0 H_i \cong 10$ T, l_C is quite close to the size of the particle, in qualitative agreement with the previous observations in Fig. 8(a).

This can also be seen in Figs. 9 and 10, where we plot, respectively, l_C and $C(r)$ for the uniform core-shell model at fixed applied magnetic fields and as a function of the ratio H_{p1}/H_{p2}. At the smaller applied fields, here, a few tesla, the largest l_C values are obtained in the hard interface region $(H_{p1}/H_{p2} < 1)$ and then l_C smoothly decreases with increasing ratio H_{p1}/H_{p2}. By contrast, for applied fields on the order of a few 10 T, the spin-misalignment lengths exhibit a tendency to decrease at the smallest H_{p1}/H_{p2} values, and the l_C take on a maximum at some intermediate value of H_{p1}/H_{p2}. This scenario is further illustrated in Fig. 10, where the respective point of intersection of the (normalized) correlation function with the horizontal line marks the corresponding value of l_C.

VII. CONCLUSIONS AND OUTLOOK

Using linearized micromagnetic theory, we have numerically computed the autocorrelation function $C(r)$ of the spin misalignment for a model system which consists of an isolated spherical nanoparticle (core-shell particle) that is embedded in an anisotropy-field-free matrix. This approach is expected to be representative for a magnetic microstructure which is characterized by an ensemble of statistically uncorrelated defects (random anisotropy). For different spatial profiles of the particle's anisotropy field (uniform sphere, uniform core shell, linear increase, and exponential and power-law decay), we have evaluated the magnetization response and from the field-dependent $C(r)$ data the associated characteristic decay length l_C of the perturbation in the spin structure. In contrast to the common assumption, the spin-misalignment correlations do not decay exponentially but exhibit a more complicated functional dependency $C(r)$. Likewise, in reciprocal space, the associated spin-misalignment scattering does not follow an asymptotic q^{-4} (Porod-type) behavior. Equation (15) has been proven to represent a reasonable definition for extracting l_C from the correlation function. Except for the core-shell model with hard interfaces, we find that the rather simple expression $l_C(H_i) = \mathcal{L} + l_H(H_i)$, where $\mathcal{L}$ is a measure for the defect size (particle size), provides a very robust description for the field dependence of l_C. Within limits, this relation appears to be independent of the detailed internal structure of the anisotropy field, and the findings provide additional justification for the use of Eq. (24) in Ref. 54 for the successful description of field-dependent correlations in nanocrystalline Co and Ni.

Improvements to the present model calculation may be achieved by combining experimental SANS data with the results of full-scale 3D micromagnetic simulations; first results in this direction are reported in Ref. 61. The present approach is restricted to the high-field limit and relies on uniform values for the exchange-stiffness constant A and saturation magnetization M_s. We have considered the response of the magnetization to a single, radially symmetric defect, $H_p = H_p(r)$, which is assumed to vanish outside the defect zone. In real specimens, however, the defect symmetry might be more complex and the materials parameters may change at phase boundaries and interfaces and, therefore, boundary conditions should be taken into account.[27] In addition to the random anisotropy of the individual defects, there may be a macroscopic magnetic anisotropy superposed. Furthermore, a distribution of defect sizes may result in a smoothing of the spin-misalignment correlations. The use of numerical micromagnetics allows one to solve some of these problems, and it would become possible to take into account the full nonlinearity of Brown's equations.

From an experimental point of view, it is worth to mention that due to the recently opened up possibility to perform routinely longitudinal neutron-polarization analysis in a SANS experiment,[62,63] spin-misalignment scattering can be directly measured in the two spin-flip channels.[64] Such experiments not only eliminate the unwanted nuclear background signal but permit the determination of partial correlation functions.[65]

ACKNOWLEDGMENTS

We thank Frank Döbrich and Rainer Birringer for fruitful discussions and for critically reading the manuscript. This research was financially supported by the Deutsche Forschungsgemeinschaft (Grants No. MI 738/3-2 and No. MI 738/6-1) and by the National Research Fund of Luxembourg in the framework of the ATTRACT project FNR/A09/01.

*andreas.michels@uni.lu

[1] M. Laver, E. M. Forgan, S. P. Brown, D. Charalambous, D. Fort, C. Bowell, S. Ramos, R. J. Lycett, D. K. Christen, J. Kohlbrecher, C. D. Dewhurst, and R. Cubitt, Phys. Rev. Lett. **96**, 167002 (2006).

[2] M. Bischof, P. Staron, A. Michels, P. Granitzer, K. Rumpf, H. Leitner, C. Scheu, and H. Clemens, Acta Mater. **55**, 2637 (2007).

[3] J. F. Löffler, H. B. Braun, W. Wagner, G. Kostorz, and A. Wiedenmann, Phys. Rev. B **71**, 134410 (2005).

[4] A. Michels, C. Vecchini, O. Moze, K. Suzuki, P. K. Pranzas, J. Kohlbrecher, and J. Weissmüller, Phys. Rev. B **74**, 134407 (2006).

[5] T. Thomson, S. L. Lee, M. F. Toney, C. D. Dewhurst, F. Y. Ogrin, C. J. Oates, and S. Sun, Phys. Rev. B **72**, 064441 (2005).

[6] M. Sachan, C. Bonnoit, S. A. Majetich, Y. Ijiri, P. O. Mensah-Bonsu, J. A. Borchers, and J. J. Rhyne, Appl. Phys. Lett. **92**, 152503 (2008).

[7] R. García Calderón, L. Fernández Barquín, S. N. Kaul, J. C. Gómez Sal, P. Gorria, J. S. Pedersen, and R. K. Heenan, Phys. Rev. B **71**, 134413 (2005).

[8] S. V. Grigoriev, D. Chernyshov, V. A. Dyadkin, V. Dmitriev, S. V. Maleyev, E. V. Moskvin, D. Menzel, J. Schoenes, and H. Eckerlebe, Phys. Rev. Lett. **102**, 037204 (2009).

[9] S. Mühlbauer, B. Binz, F. Jonietz, C. Pfleiderer, A. Rosch, A. Neubauer, R. Georgii, and P. Böni, Science **323**, 915 (2009).

[10] A. Wiedenmann, U. Keiderling, K. Habicht, M. Russina, and R. Gähler, Phys. Rev. Lett. **97**, 057202 (2006).

[11] K. Mortensen and J. S. Pedersen, Macromolecules **26**, 805 (1993).

[12] A. Kahle, B. Winkler, A. Radulescu, and J. Schreuer, Eur. J. Mineral. **16**, 407 (2004).

[13] A. Blanchard, R. S. Graham, M. Heinrich, W. Pyckhout-Hintzen, D. Richter, A. E. Likhtman, T. C. B. McLeish, D. J. Read, E. Straube, and J. Kohlbrecher, Phys. Rev. Lett. **95**, 166001 (2005).

[14] R. Willumeit, N. Burkhardt, R. Jünemann, J. Wadzack, K. H. Nierhaus, and H. B. Stuhrmann, J. Appl. Crystallogr. **30**, 1125 (1997).

[15] V. K. Aswal, S. Chodankar, J. Kohlbrecher, R. Vavrin, and A. G. Wagh, Phys. Rev. E **80**, 011924 (2009).

[16] A. Wiedenmann, in *Ferrofluids: Magnetically Controllable Fluids and Their Applications*, Lecture Notes in Physics, edited by S. Odenbach (Springer, Berlin, 2002), pp. 33–58.

[17] D. I. Svergun and M. H. J. Koch, Rep. Prog. Phys. **66**, 1735 (2003).

[18] H. B. Stuhrmann, Rep. Prog. Phys. **67**, 1073 (2004).

[19] W. Wagner and J. Kohlbrecher, in *Modern Techniques for Characterizing Magnetic Materials*, edited by Y. Zhu (Kluwer Academic, Boston, 2005), pp. 65–103.

[20] Y. B. Melnichenko and G. D. Wignall, J. Appl. Phys. **102**, 021101 (2007).

[21] A. Michels and J. Weissmüller, Rep. Prog. Phys. **71**, 066501 (2008).

[22] A. Guinier and G. Fournet, *Small-Angle Scattering of X-Rays* (Wiley, New York, 1955).

[23] *Small-Angle X-Ray Scattering*, edited by O. Glatter and O. Kratky (Academic Press, London, 1982).

[24] S.-H. Chen and T.-L. Lin, in *Methods of Experimental Physics–Neutron Scattering, Part B*, edited by D. L. Price and K. Sköld (Academic Press, San Diego, 1987), Vol. 23, pp. 489–543.

[25] J. S. Pedersen, Adv. Colloid Interface Sci. **70**, 171 (1997).

[26] P. G. de Gennes, in *Magnetism*, edited by G. T. Rado and H. Suhl (Academic Press, New York, 1963), Vol. 3, pp. 115–147.

[27] R. Skomski, J. Phys.: Condens. Matter **15**, R841 (2003).

[28] I. Dzyaloshinsky, J. Phys. Chem. Solids **4**, 241 (1958).

[29] T. Moriya, Phys. Rev. **120**, 91 (1960).

[30] M. Bode, M. Heide, K. von Bergmann, P. Ferriani, S. Heinze, G. Bihlmayer, A. Kubetzka, O. Pietzsch, S. Blügel, and R. Wiesendanger, Nature (London) **447**, 190 (2007).

[31] S. V. Grigoriev, Y. O. Chetverikov, D. Lott, and A. Schreyer, Phys. Rev. Lett. **100**, 197203 (2008).

[32] W. F. Brown, Jr., *Micromagnetics* (Interscience, New York, 1963).

[33] S. Shtrikman and D. Treves, in *Magnetism*, edited by G. T. Rado and H. Suhl (Ref. 26), Vol. 3, pp. 395–414.

[34] A. Aharoni, *Introduction to the Theory of Ferromagnetism*, 2nd ed. (Clarendon Press, Oxford, 1996).

[35] H. Kronmüller and M. Fähnle, *Micromagnetism and the Microstructure of Ferromagnetic Solids* (Cambridge University Press, Cambridge, 2003).

[36] See, e.g., *Handbook of Magnetism and Advanced Magnetic Materials: Micromagnetism*, edited by H. Kronmüller and S. Parkin (Wiley, Chichester, 2007), Vol. 2.

[37] J. Blin, Acta Metall. **5**, 528 (1957).

[38] A. Seeger, Acta Metall. **5**, 24 (1957).

[39] H. H. Atkinson, Philos. Mag. **3**, 476 (1958).

[40] A. K. Seeger, J. Appl. Phys. **30**, 629 (1959).

[41] H. Kronmüller, A. Seeger, and M. Wilkens, Z. Phys. **171**, 291 (1963).

[42] W. Vorbrugg and O. Schärpf, Philos. Mag. **32**, 629 (1975).

[43] W. Vorbrugg, Philos. Mag. **32**, 643 (1975).

[44] G. Göltz, H. Kronmüller, A. Seeger, H. Scheuer, and W. Schmatz, Philos. Mag. A **54**, 213 (1986).

[45] T. Schrefl, J. Fidler, and H. Kronmüller, Phys. Rev. B **49**, 6100 (1994).

[46] M. Bachmann, R. Fischer, and H. Kronmüller, in *Magnetic Anisotropy and Coercivity in Rare-Earth Transition Metal Alloys*, edited by L. Schultz and K.-H. Müller (Werkstoff-Informationsgesellschaft, Frankfurt, 1998), pp. 217–236.

[47] D. V. Berkov and N. L. Gorn, Phys. Rev. B **57**, 14332 (1998).

[48] R. Hertel and H. Kronmüller, Phys. Rev. B **60**, 7366 (1999).

[49] A. Thiaville, J. M. García, R. Dittrich, J. Miltat, and T. Schrefl, Phys. Rev. B **67**, 094410 (2003).

[50] A. Thiaville, Y. Nakatani, F. Piéchon, J. Miltat, and T. Ono, Eur. Phys. J. B **60**, 15 (2007).

[51] A. Vansteenkiste, M. Weigand, M. Curcic, H. Stoll, G. Schütz, and B. V. Waeyenberge, New J. Phys. **11**, 063006 (2009).

[52] J. Weissmüller, A. Michels, J. G. Barker, A. Wiedenmann, U. Erb, and R. D. Shull, Phys. Rev. B **63**, 214414 (2001).

[53] A. Guinier, *X-Ray Diffraction in Crystals, Imperfect Crystals, and Amorphous Bodies* (Dover, New York, 1994), p. 31.

[54] A. Michels, R. N. Viswanath, J. G. Barker, R. Birringer, and J. Weissmüller, Phys. Rev. Lett. **91**, 267204 (2003).

[55] J. Weissmüller, A. Michels, D. Michels, A. Wiedenmann, C. E. Krill III, H. M. Sauer, and R. Birringer, Phys. Rev. B **69**, 054402 (2004).

[56] F. Döbrich, M. Elmas, A. Ferdinand, J. Markmann, M. Sharp, H. Eckerlebe, J. Kohlbrecher, R. Birringer, and A. Michels, J. Phys.: Condens. Matter **21**, 156003 (2009).

[57] G. Porod, in *Small-Angle X-Ray Scattering*, edited by O. Glatter and O. Kratky (Ref. 23), pp. 17–51.

[58] G. Walter, R. Kranold, T. Gerber, J. Baldrian, and M. Steinhart, J. Appl. Crystallogr. **18**, 205 (1985).

[59] F. Dolcini, L. Ferrari, A. Rioli, and C. Degli Esposti Boschi, Phys. Rev. E **57**, 2594 (1998).

[60] H. Kronmüller and A. Seeger, J. Phys. Chem. Solids **18**, 93 (1961).

[61] S. Saranu, A. Grob, J. Weissmüller, and U. Herr, Phys. Status Solidi A **205**, 1774 (2008).

[62] U. Keiderling, A. Wiedenmann, A. Rupp, J. Klenke, and W. Heil, Meas. Sci. Technol. **19**, 034009 (2008).

[63] K. L. Krycka, R. Booth, J. A. Borchers, W. C. Chen, C. Conlon, T. R. Gentile, C. Hogg, Y. Ijiri, M. Laver, B. B. Maranville, S. A. Majetich, J. J. Rhyne, and S. M. Watson, Physica B **404**, 2561 (2009).

[64] R. M. Moon, T. Riste, and W. C. Koehler, Phys. Rev. **181**, 920 (1969).

[65] D. Honecker, A. Ferdinand, F. Döbrich, C. D. Dewhurst, A. Wiedenmann, C. Gómez-Polo, K. Suzuki, and A. Michels, Eur. Phys. J. B **76**, 209 (2010).